Defect imaging in composite structures

Paul Fromme, Marco Endrizzi, and Alessandro Olivo

Articles you may be interested in

The optical lens coupled X-ray in-line phase contrast imaging system for the characterization of low Z materials
Review of Scientific Instruments **89**, 053703 (2018); 10.1063/1.5019830

Trochoidal X-ray Vector Radiography: Directional dark-field without grating stepping
Applied Physics Letters **112**, 111902 (2018); 10.1063/1.5020361

Stabilising high energy orbit oscillations by the utilisation of centrifugal effects for rotating-tyre-induced energy harvesting
Applied Physics Letters **112**, 143901 (2018); 10.1063/1.5019907

Application of wavefield imaging to characterize scattering from artificial and impact damage in composite laminate panels
AIP Conference Proceedings **1949**, 090007 (2018); 10.1063/1.5031570

Development of eddy current probe for fiber orientation assessment in carbon fiber composites
AIP Conference Proceedings **1949**, 120004 (2018); 10.1063/1.5031591

Guided ultrasonic wave beam skew in silicon wafers
AIP Conference Proceedings **1949**, 090005 (2018); 10.1063/1.5031568

Defect imaging in composite structures

Paul Fromme[1a], Marco Endrizzi[2], Alessandro Olivo[2]

[1] *Department of Mechanical Engineering, University College London, United Kingdom*
[2]*Department of Medical Physics and Biomedical Engineering, UCL, United Kingdom*

[a]pfromme@ucl.ac.uk

Abstract. Carbon fiber laminate composites offer advantages including a good strength to weight ratio for aerospace structures. However, manufacturing imperfections and impact during the operation and servicing of the aircraft can lead to barely visible and difficult to detect damage. Incorrect ply lay-up during the manufacturing process can result in fiber misalignment or in-plane and out-of-plane waviness. Impact, such as bird strike, during the service life can lead to delamination and cracking, reducing the load carrying capacity of the structure. Both ultrasonic and X-ray techniques have a good track record for the nondestructive testing of composite structures; for the latter, phase-based approaches provide additional advantages due to their enhanced sensitivity. Bulk and guided ultrasonic waves propagating in the composite panel were employed for defect imaging. Ultrasonic immersion C-scans of a composite panel with barely visible impact damage were taken to characterize the size and shape of damage (delamination). The first antisymmetric A_0 Lamb wave mode was excited experimentally using piezoelectric transducers and measured using a laser vibrometer. X-ray phase-contrast and dark field imaging, implemented through the edge-illumination (EI) approach, were used for the detailed visualization of the damages in the composite material. The Edge-illumination approach is multi-modal and provides three representations of the sample: absorption, differential phase and dark-field. The latter is of particular interest to detect cracks and voids of dimensions that are smaller than the actual spatial resolution of the imaging system. Application examples for carbon fiber composite plates with barely visible impact damage are shown.

INTRODUCTION

In the aerospace industry composite materials are widely used as they offer beneficial strength to weight capacity. However, impact loading can lead to barely visible damage [1]. Hidden failure modes such as matrix cracks, fiber damage, and delaminations can reduce the integrity and load bearing capacity of the structure [2]. A range of non-destructive testing methods are utilized for post-manufacture and in-service inspection and monitoring of composite components [3, 4]. Bulk wave ultrasound has been demonstrated to have good sensitivity for the detection of out-of-plane ply wrinkling, in-plane fiber orientation and porosity in composites [5]. Ultrasonic immersion C-scans allow for accurate measurements of the location and size of damage, especially for delaminations [6-8]. Guided ultrasonic waves can be employed for efficient monitoring of large structures [9]. High frequency guided waves have been successfully used to detect damage such as fatigue cracks in metallic structures [10, 11]. The propagation of guided ultrasonic waves in composite plates is direction dependent due to the anisotropic material properties [12]. Coupled with high attenuation values for composite materials, inspection using higher guided wave modes is difficult. Employing a single guided wave mode at low frequency has been found to be advantageous to avoid complications. The capacity of guided ultrasonic waves for delamination detection [13, 14] in composite structures was demonstrated. The scattering of the first anti-symmetric guided wave mode (A_0) at impact damage in composite panels was measured experimentally and compared to Finite Element simulations [15].

X-ray methods have been employed successfully for the detection of internal defects [16], often using dye penetrant to overcome the limited X-ray contrast in carbon fiber composites [17]. 3D visualization and characterization of composite damage, including voids and micro cracking, was achieved using Micro CT scans [18]. Detailed 3D models of damaged composite components were developed using C-scan and CT scan data [19]. Conventional radiography can be extended using X-ray phase-contrast imaging (XPCI) methods for applications where low-contrast details have to be observed non-destructively [20]. Recent reviews on the subject provide details of the imaging methods, developments and their applications [21]. Edge-illumination (EI) and its area-imaging implementation sometimes referred to as "coded-aperture" [22], are XPCI techniques enabling quantitative amplitude and phase retrieval [23], as well as "dark-field" approaches [24], which are particularly well suited to the detection of inhomogeneities on the microscopic scale, like those that could be created by an impact on a previously homogeneous material. EI can be adapted for use with rotating anode [22] and microfocal [25] X-ray tubes, notably, making it particularly attractive for use with compact, laboratory-scale equipment.

This contribution presents the complimentary imaging results for a cross-ply composite plate with barely visible impact damage using ultrasonic immersion C-scans, guided ultrasonic waves, and EI differential phase and dark-field methods for the visualization of defects [26]. The sample, the ultrasonic C-scan and guided wave setup and the phase-based X-ray imaging system are described. The images obtained by means of such systems are presented and compared to show the complementarity of these techniques.

EXPERIMENTS

Composite Specimen

The specimen had been manufactured and previously investigated by the Composite Systems Innovation Centre, University of Sheffield [1]. The composite component (size: 990 mm x 110 mm) was fabricated with unidirectional pre-pregs using autoclave cure of Cytec 977-2/ Tenax HTS cross-ply laminates. The plate consists of 8 pre-preg layers with a symmetric layup sequence of $[0/90]_{2s}$, giving a thickness of 2 mm. Using standard drop weight impact procedures, the specimen was subjected to a 7.4 J impact damage using a hemispherical 15 mm impactor head. A small degree of fiber fracture and indentation on the surface of the plate can be seen marked in Fig. 1.

Ultrasonic Immersion C-scan

Immersion ultrasonic C-scans were performed to obtain information about the impact damage in the defective composite plates. The plate was cut to 200 mm length, keeping the 110 mm width. A 10 MHz unfocused ultrasonic transducer with quarter inch diameter was mounted perpendicular to the surface of the plate on a computer-controlled scanning rig. The scanned area was 80 mm x 40 mm with a step size of 1 mm in both directions. The pulse-echo signal for each scan point was acquired using a digital oscilloscope (500 time points, sampling frequency 100 MHz) and analyzed using MATLAB. A double-through transmission scan was performed with time-gate set around the pulse reflected at a 12 mm thick steel plate, placed 5 mm below the composite plate in the water bath, and the maximum amplitude for each scan point extracted. Another C-scan was conducted to record the negative minimum amplitude that corresponds to the ultrasonic pulse reflected within the composite specimen with appropriate time gating.

FIGURE 1. Photograph of composite specimen with barely visible impact damage marked.

Guided Ultrasonic Waves

The scattered guided ultrasonic wave field around the impact damage location on the composite specimen was measured experimentally. A piezoelectric transducer (piezoelectric disc of 5 mm diameter and 2 mm thickness, brass backing mass of 5 mm diameter and 6 mm thickness) was bonded to the plate approximately 50 mm from the center of the impact damage. The first anti-symmetrical (A_0) guided wave mode was excited as a 5-cycle Hanning windowed tone-burst with a center frequency of 100 kHz, generated by a programmable function generator. The wave propagation was recorded using a heterodyne laser vibrometer fixed to a scanning rig and moved parallel to the specimen. The scanned area was 80 mm x 40 mm with a step size of 1 mm in both directions. The time traces of the received signals were filtered using a band pass filter (75 – 125 kHz) and were recorded and averaged (20 averages) using a digital storage oscilloscope. All signals were transferred to a PC and analyzed using Matlab. The maximum amplitude at each measurement point was extracted using the Hilbert transform.

X-ray Imaging

The experimental set-up for an EI phase-based x-ray imaging system consists of an X-ray source, a sample mask that shapes the beam before it interacts with the sample, a second mask used as a beam "analyzer" and a digital detector [22]. Detailed parameters used for this experiment are given in reference [26]. The setup had a geometrical magnification of 1.25. The source was a molybdenum target, rotating anode X-ray tube. A description of image formation for a typical laboratory set-up is given in reference [23]. The measured intensity at the detector can be seen as the convolution between the sample and the system "illumination function", obtained by scanning one mask with respect to the other in the absence of a sample. This function describes how the detected X-ray intensity changes as a function of the lateral shift between the two masks: it is maximum when the sample and the detector aperture are perfectly aligned and it gradually decreases as the lateral shift between the two apertures becomes larger. In order to retrieve the sample properties from the convolution equation, the parameters describing the sample are iteratively refined, and corrected for the inaccuracies arising from the masks' imperfections [27]. This allows the calculation of images characterizing the absorption, refraction, and dark-field related to changes in the specimen properties.

ULTRASONIC C-SCAN

The amplitudes of the double-through transmission and reflection C-scans of the composite specimen are shown in Fig. 2. The impact center was at approximately 50 mm in the x-direction and 20 mm in the y-direction. For the double-through transmission (Fig. 2 top) an area with distinctive low amplitude (dark blue) can be identified, extending about 60 mm in the x-direction and 25 mm in the y-direction. This indicates the delamination area, as the amplitude of the ultrasonic pulse transmitted twice across the delamination is significantly reduced. In the area around the delamination a pattern of higher amplitudes (yellow) can be observed. This pattern is linked to the specimen surface and internal structure, leading to variations in the ultrasonic transmission and reflection. Lines of low amplitude can be identified at 35 and 50 mm in the x-direction and about 35 mm in the y-direction, which could be linked to damage extending along the cross-ply fiber directions.

Figure 2 bottom shows the reflected amplitude (negative) of the second C-scan from the composite plate. The size and shape of the area of large negative amplitude matches well with the delamination observed for the double-through transmission above. The area of lower (negative) amplitude around 55 mm in the x-direction and 25 mm in the y-direction corresponds to a small indent visible from the drop-weight impact location (Fig. 1). It can be clearly observed that the delamination area is not symmetric around the center of the impact, extending significantly further to the left along the x-axis. The observed delamination shape exhibits a less regular pattern than previously found in literature [19]. Due to the chosen ultrasonic center frequency at 10 MHz, insufficient resolution in the thickness direction was available to obtain accurate depth information of the delamination damage. The area around the delamination again shows a pattern corresponding to the composite plate structure, with larger negative amplitude (40 - 70 mm in x-direction) potentially corresponding to different composite damage mechanisms.
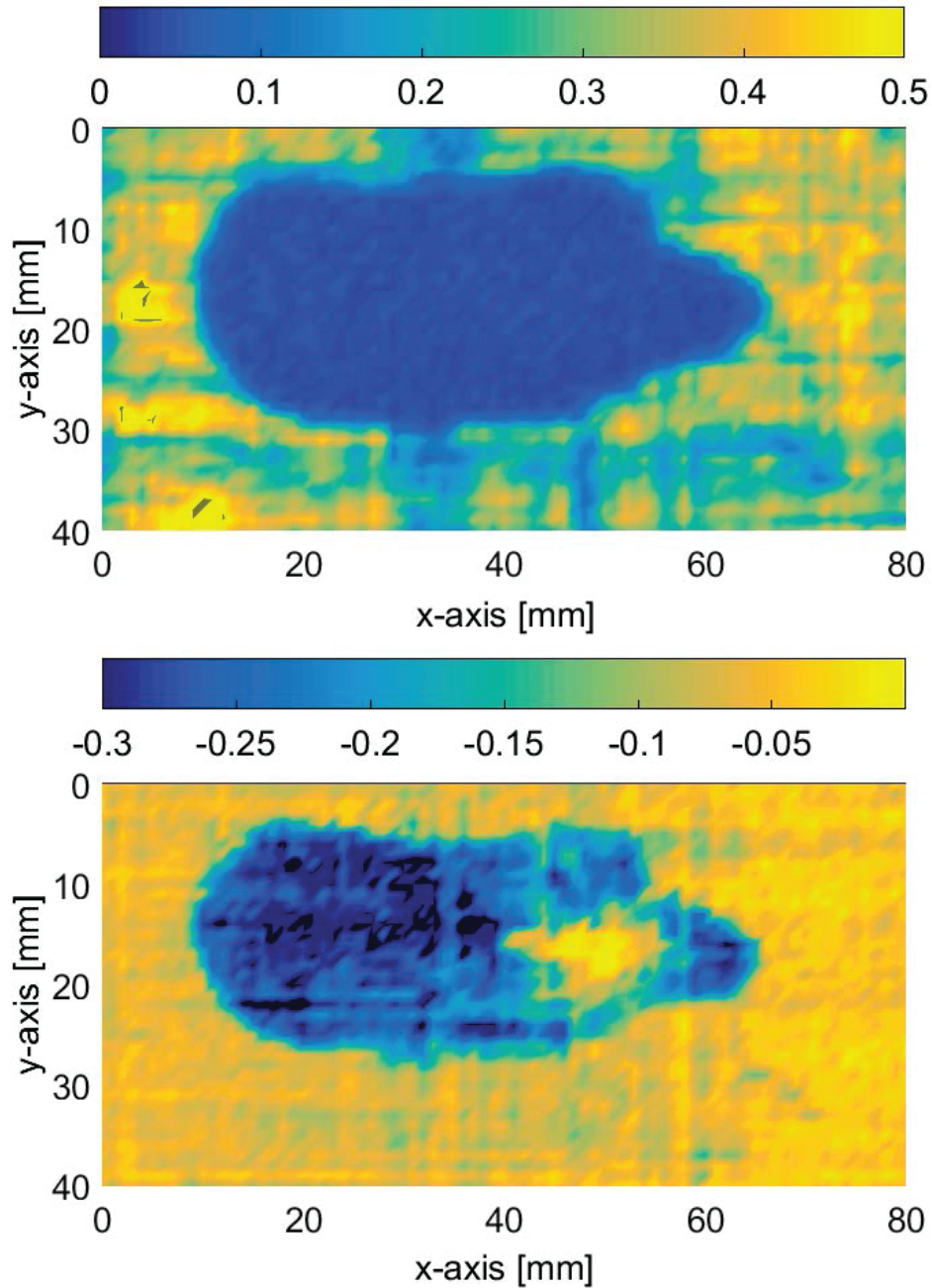
FIGURE 2. Ultrasonic C-scan images of damage in composite specimen; maximum amplitude of time-gated signal, 10 MHz immersion transducer, 1 mm step size; top: double-through transmission; bottom: pulse reflection.

GUIDED ULTRASONIC WAVE IMAGING

The amplitude of the guided ultrasonic wave field is shown in Fig. 3. Please note that the x- and y-directions are swapped as compared to Fig. 2. The fixed excitation transducer is placed at -30 mm in the negative x-direction, so that the incident wave is propagating in the positive x-direction. The guided wave measurements use a different experimental configuration compared to the immersion C-Scan, with a fixed excitation transducer and a laser head scanned over a grid with the same resolution, but centered on the impact location, to record the signal amplitude at each measurement point.
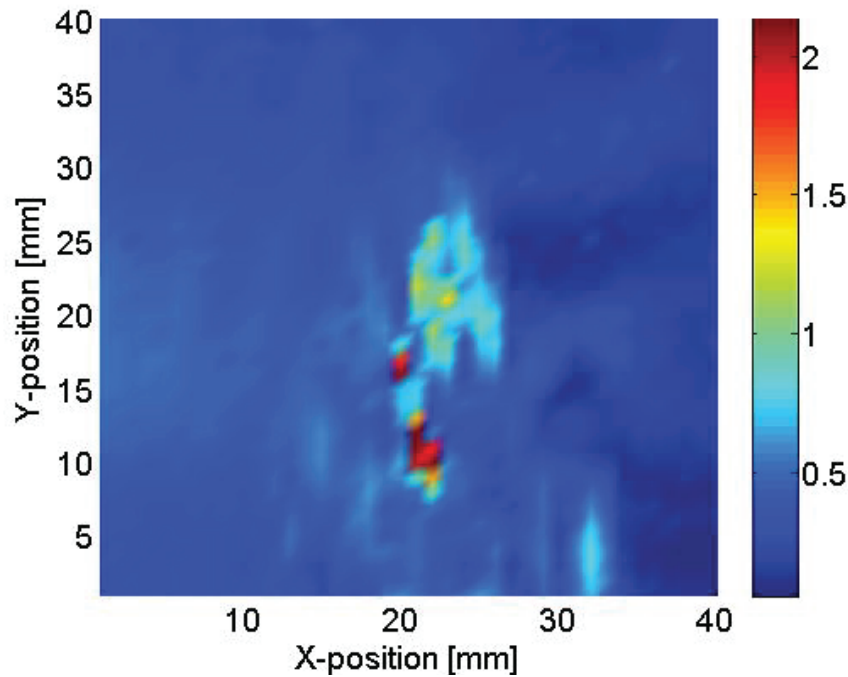
FIGURE 3. Amplitude of guided ultrasonic wave field scattered at impact damage in composite specimen, 100 kHz excitation, transducer at -30 mm in negative x-direction (incident wave propagation in positive x-direction), 1 mm step size, maximum amplitude of time trace at each scan position.

The incident wave field shows higher amplitude along the fiber direction (around x = 0 mm, y = 20 mm) as expected for an anisotropic composite plate. At the center of the impact damage (x = 20 mm, y = 10-30 mm) very high amplitudes can be observed. This is the area where visually the small indent from the drop weight was observed and where the reflection immersion C-scan showed a change in the reflected ultrasonic amplitude. In addition to the delamination caused by the impact, further damage of the composite structure appears to have occurred. In literature, matrix cracking and fiber breakage at the impact center has been reported. An area with increased amplitude can be observed from approximately 10 to 32 mm in the x-direction and 0 to 30 mm in the y-direction. While no specific registration relative to the immersion C-scan measurements was done, this approximately coincides with the delamination area observed in Fig. 2 (rotated by 90 degrees). In the guided wave propagation direction behind the defect (from about x = 30 mm) lower amplitude of the guided wave can be observed. This is due to the scattering of the guided wave at the impact damage with limited energy propagated past the damage location. In general, good agreement of the damage extent with the immersion ultrasonic C-scans was observed. However, even though both are ultrasonic methods, the wave propagation direction and characteristics are different, so the two methods are sensitive to different aspects of the impact damage in composite structures.

X-RAY EDGE ILLUMINATION PHASE-BASED IMAGING

The different images obtained from the EI X-ray phase contrast imaging are shown in Fig. 4, where conventional radiography (top), differential phase image (center) and dark-field image (bottom) are compared. Left and right columns show the composite specimen rotated by 90° as the EI X-ray phase contrast imaging is sensitive to the orientation of the damage relative to the masks' apertures, which are effectively long slits. The conventional radiography images (Fig. 4 top) show some of the inner structure of the composite specimen, but damage is not visible. It should be noted that no dye penetrant was used. Damage of the plate structure, close to the impact location center, can be seen in the dark-field images (Fig. 4 bottom) and is pointed out by the red arrows. Different damage extent along the respective fiber directions can be observed in the two dark-field images, which were acquired by rotating the specimen by 90° around the X-ray beam axis.
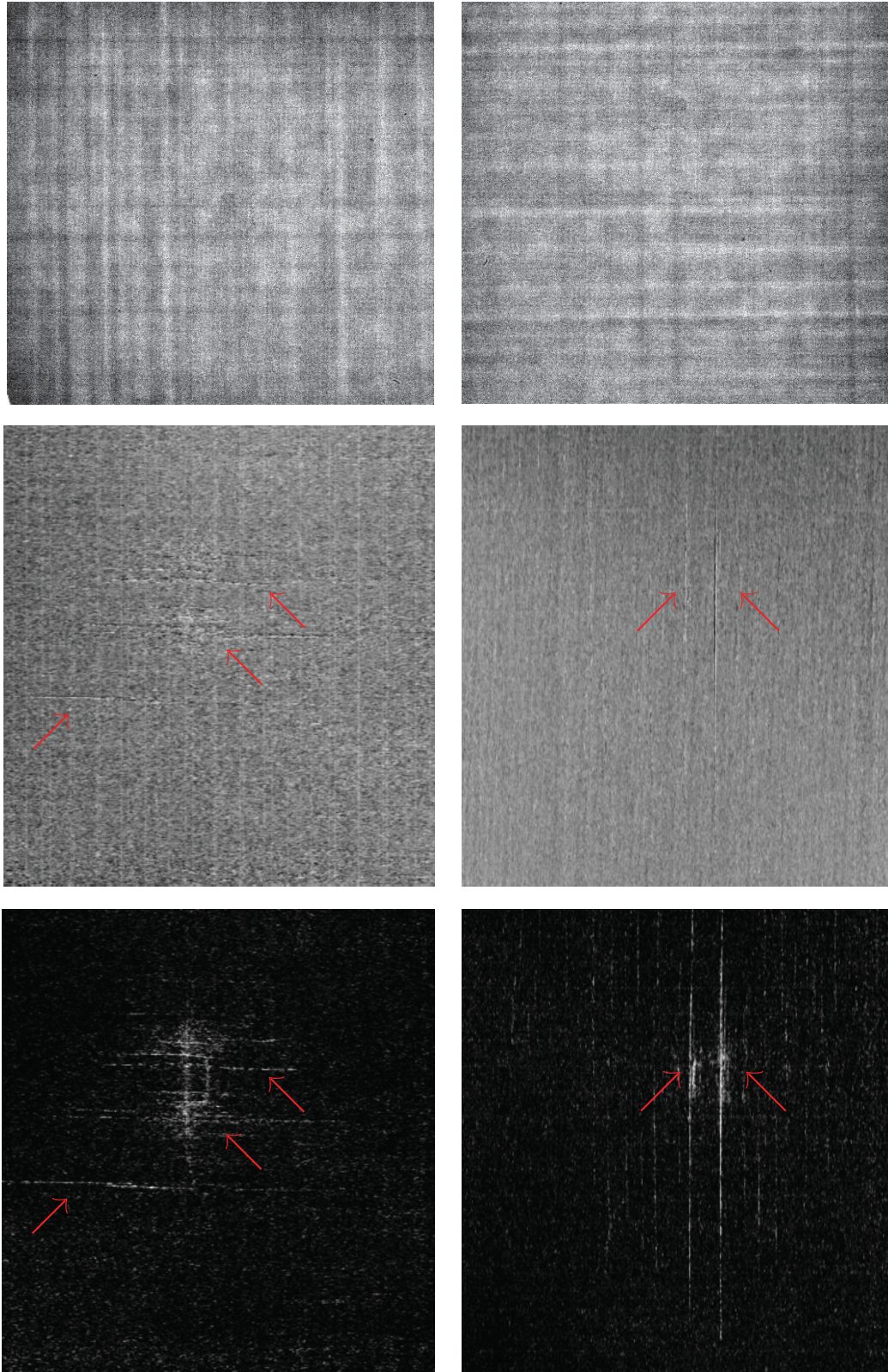
FIGURE 4. X-ray images of damage in composite specimen; top: conventional radiography; center: differential phase; bottom: dark-field image; left: horizontal; right: vertical rotation of specimen around X-ray beam axis.

This demonstrates the various damage orientations along the direction of the fibers in the cross-ply structure, both in the width and length direction of the specimen. The EI imaging technique has the property that the signal appears modulated by the angle between specific sample features and the relative orientation of the optical mask apertures. Maximum signal is obtained when these are aligned, with minimum signal when orthogonal. The dependence of the sensitivity to the damage orientation could be further exploited to improve the characterization and modelling of the impact damage in composite plates. For different lay-up configuration, e.g., a quasi-isotropic plate, further measurements could easily be conducted in the +/- 45° fiber directions.

The longer damage is also visible in the differential phase image (Fig. 4 center), illustrated by the arrows. The visibility from the images is not as clear as for the dark-field images (Fig. 4 bottom) for this case of impact damage, and only features aligned with the direction of the aperture are visible. The X-ray EI images, especially the dark-field imaging, are sensitive to damage along the fiber directions aligned with the system aperture and typically on a smaller length scale than the ultrasonic images, which are to some degree limited by the ultrasonic wavelength.

CONCLUSIONS

Impact damage in composite structures leads to a range of damage mechanism over different length scales, ranging from matrix cracks and fiber debonding to delaminations. Nondestructive testing is essential for aerospace components to detect and quantify manufacturing and in-service damage and to ensure safe operation. This contribution compared three methods based on conventional immersion ultrasound C-scans, guided ultrasonic waves and phase-based X-ray imaging implemented via the Edge Illumination approach. For a cross-ply composite specimen with barely visible impact damage, the double-through immersion C-scan showed good sensitivity to quantify the delamination size and shape. From an additional immersion C-scan based on reflected amplitude at features within the specimen, both the delamination and additional internal damage and structure of the composite specimen could be observed. Guided ultrasonic wave measurements conducted at a significantly lower excitation frequency and thus larger ultrasonic wavelength showed high amplitudes within the damaged area and a significant amplitude drop behind the defect. In general, a good correlation of the observed damage extent to the immersion C-scans was found. The X-ray Edge Illumination phase-based imaging is sensitive to damage on a smaller scale and has a direction-dependent sensitivity for the orientation of the sample with respect to the X-ray system and masks. Small scale damage extending along the fiber directions could be clearly observed, especially in the dark-field images. The complementary nondestructive testing and imaging methods allowed for a good characterization of the impact damage in the cross-ply composite specimen. Further measurements for different levels of impact severity and composite specimens with improved image registration would allow for a better quantification of defect types and the respective sensitivity of the nondestructive testing methods.

ACKNOWLEDGMENTS

REFERENCES

1. T.J. Swait, F.R. Jones, and S.A. Hayes, *Compos. Sci. Technol.* **72**, 1515-1523 (2012).
2. M.O.W. Richardson and M.J. Wisheart, *Compos.* Part A **27**, 1123-1131 (1996).
3. I. Scott and C. Scala, *NDT Int.* **15**, 75-86 (1982).
4. I. Amenabar, A. Mendikute, A. López-Arraiza, M. Lizaranzu, and J. Aurrekoetxea, *Compos.* Part B: Eng. **42**, 1298-1305 (2011).
5. R. Smith, L. Nelson, N. Xie, C. Fraij, and S. Hallett, *Insight* **57**,131-139 (2015).
6. D. Kiefel, R. Stoessel, and C. Grosse, *AIP Conf Proc* **1650**, 591-598 (2015).
7. P. Lloyd, *Ultrasonics* **27**, 8-18 (1989).

8. D.D. Symons, *Compos. Sci. Technol.* **60**, 391-401 (2000).
9. J.S. Hall, P. Fromme, and J.E. Michaels, *J. Nondestruct. Eval.* **33**, 299-308 (2014).
10. B. Masserey and P. Fromme, *NDT&E Int.* **71**, 1-7 (2015).
11. B. Masserey and P. Fromme, *Insight* **51**, 667-671 (2009).
12. M. Castaings and B. Hosten, *J. Acoust. Soc. Am.* **113**, 2622-2634 (2003).
13. N. Toyama and J. Takatsubo, *Compos. Sci. Technol.* **64**, 1293-1300 (2004).
14. K. S. Tan, N. Guo, B. S. Wong, and C.G. Tui, *Compos. Sci. Technol.* **53**, 77-84 (1995).
15. B.I.S. Murat, P. Khalili, and P. Fromme, *J. Acoust. Soc. Am.* **139**, 3044-3052 (2016).
16. P. Lloyd, *Ultrasonics* **27**, 8-18 (1989).
17. J.A. Lavoie and E. Adolfsson, *J Compos. Mater.* **35**, 2077-2097 (2001).
18. P.J. Schilling, B.R. Karedla, A.K. Tatiparthi, M.A. Verges, and P.D. Herrington, *Compos. Sci. Technol.* **65**, 2071-2078 (2005).
19. C.A. Leckey, M.D. Rogge, and F.R. Parker, *Ultrasonics* **54**, 385-394 (2014).
20. R. Fitzgerald, Phys. Today **53**, 23–26 (2000).
21. A. Olivo and E. Castelli, *Riv. Nuovo Cimento* **37**, 467-508 (2014).
22. A. Olivo and R. Speller, *Appl. Phys. Lett.* **91**, 074106 (2007).
23. P.R. Munro, K. Ignatyev, R.D. Speller, and A. Olivo, *Proc. Natl. Acad. Sci. USA* **109**, 13922-13927 (2012).
24. M. Endrizzi, P.C. Diemoz, T. P. Millard, J.L. Jones, R.D. Speller, I.K. Robinson, and A. Olivo, *Appl. Phys. Lett.* **104**, 024106 (2014).
25. M. Endrizzi, F.A. Vittoria, P.C. Diemoz, R. Lorenzo, R.D. Speller, U.H. Wagner, C. Rau, I.K. Robinson, A. Olivo, *Opt. Lett.* **39**, 3332-3335 (2014).
26. M. Endrizzi, B.I.S. Murat, P. Fromme, and A. Olivo, *Compos. Struct.* **134**, 895-899 (2015).
27. M. Endrizzi and A. Olivo, *J. Phys. D: Appl. Phys.* **47**, 505102 (2014).